ACS SENSORS

pubs.acs.org/acssensors
Article

Mid-Infrared Quantum Cascade Laser Sensor System with Molecularly Imprinted Polymer Solid Phase Enrichment for Diclofenac Monitoring

Sherman Lesly Zambou Jiokeng,* Dionysis Adamou, Amelie Huber, Lauralie Debard, Giorgos Katsouras, Panagiotis Georgiadis, Miltiadis Vasileiadis, Anthi Yfanti, Zoe Zacharouli, Panagiotis Margaritis, and Boris Mizaikoff*

Cite This: https://doi.org/10.1021/acssensors.6c01927

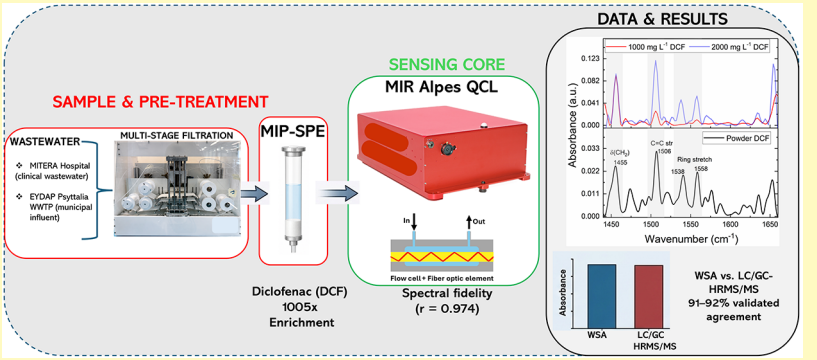

ABSTRACT: Real-time monitoring of pharmaceutical micropollutants in wastewater remains challenging due to complex matrices and low target concentrations, limiting timely detection of emerging contaminants. We report a field-deployable wastewater spectroscopic analyzer (WSA) that combines mid-infrared quantum cascade laser spectroscopy (QCL) absorption spectroscopy with selective sample preconcentration to quantitatively identify diclofenac (DCF), a widely used anti-inflammatory drug and recognized EU priority pollutant, in wastewater. Raw samples are first filtered to remove particulates, then selectively concentrated using a diclofenac-molecularly imprinted polymer-based solid phase extraction (MIP-SPE), and finally eluted as a methanol solution into a mid-infrared flow cell for spectral quantification. This integrated workflow enables autonomous operation with minimal manual intervention, addressing a key limitation of conventional laboratory-based analysis. The technique was validated against reference chromatography/mass spectrometry methods during filed deployment at a hospital and a municipal wastewater treatment plant, showing strong agreement (91–92%) and confirming its potential as a practical tool for autonomous, real-time pharmaceutical surveillance and early-warning monitoring in wastewater.

KEYWORDS: *quantum cascade laser, mid-infrared spectroscopic, diclofenac, molecularly imprinted polymer, wastewater monitoring, solid-phase extraction, field-deployable sensor*

Water quality is a critical environmental and public health concern, with pharmaceutical residues, are increasingly reported in surface waters and wastewater effluents worldwide. Among these compounds, diclofenac (DCF), a widely used non-steroidal anti-inflammatory drug, is one of the most frequently detected pollutants in municipal and hospital wastewater due to its high consumption and incomplete removal in conventional treatment plants.[1,2] DCF concentrations in effluents can reach several μg L^{-1}, exceeding levels associated with ecotoxicological effects and motivating continuous, real-time monitoring.[3−6]

Current analytical methods primarily rely on chromatographic techniques (GC-MS, LC-MS, HPLC), which provide excellent sensitivity and selectivity but require labor-intensive sample preparation, expensive instrumentation, and centralized laboratory workflows with turnaround times of 2–5 days.[7−9] These constraints limit temporal resolution and spatial coverage, especially for dynamic point sources such as hospitals and

Received: May 5, 2026
Revised: August 1, 2026
Accepted: August 4, 2026

https://doi.org/10.1021/acssensors.6c01927
ACS Sens. XXXX, XXX, XXX−XXX

large wastewater treatment plants. Alternative optical and electrochemical sensors have been explored,[10−15] yet most platforms remain confined to controlled sensors studies and often lack the molecular-fingerprint specificity needed to unambiguously distinguish DCF from structurally related interferents in complex wastewater matrices.[2,16,17]

Mid-infrared (MIR, 3–12 μm) spectroscopy provides direct access to characteristic molecular fingerprints and has been widely applied to pharmaceutical analysis and water quality assessment.[18−22] However, conventional FTIR systems are typically bulky and laboratory-bound, limiting their deployment for on-site monitoring.[20,23,24] Quantum cascade laser (QCLs) overcome these constraints as compact, high-brightness MIR sources that enabling miniaturized, field-grade sensors with improved sensitivity and robustness.[25−28] Recent developments in MIR photonic platforms and fiber-optic interfaces further support the transition of QCL technology towards environmental sensing in challenging matrices.[29,30]

This study presents a wastewater spectroscopic analyzer (WSA), to our knowledge one of the first autonomous, field-deployable MIR-QCL sensor platforms integrating multistage filtration, diclofenac-specific molecularly imprinted polymer solid-phase extraction (MIP-SPE), and QCL detection for continuous DCF monitoring in real wastewater. The system is validated through campaigns at a hospital effluent (MITERA) and a large municipal wastewater treatment plant (EYDAP Psyttalia, Greece), demonstrating high enrichment factors, strong DCF selectivity in multi-pollutant matrices, and excellent agreement with LC/GC-HRMS/MS reference methods. By combining selective sorption preconcentration with the MIR fingerprint spectroscopy in an automated architecture, the WSA advances the technology readiness level of MIR-QCL sensing toward practical early-warning networks for EU priority pollutants in wastewater.

MATERIAL AND METHODS

Reagents and Chemicals

Diclofenac sodium (DF-Na), ethylene glycol dimethacrylate (EGDMA), (2-Hydroxypropyl)-β-cyclodextrin (HPβCD), dry triethylamine (TEA), acryloyl chloride, and the photoinitiator (1-Hydroxycyclohexyl)phenylmethanone (HCPHM) were obtained at analytical grade form commercial suppliers and used as received. Carbamazepine (CBZ), acetylsalicylic acid (ASA), ibuprofen (IBU), and organic solvents (dimethylformamide, DMSO, acetonitrile, methanol, ethanol, acetone) were purchased from standard vendors in analytical grade purity. Ultrapure water (UPW, 18.2 MΩ cm^{-1}) was produced with a Sartorius Arium® pro system. Commercial SPE hardware (empty 3 mL cartridges and polyethylene frits) was used for packing the sorbents. Detailed reagent specifications and suppliers are listed in the Supporting Information. DCF-Na was converted to its neutral acid form by acidification to pH 2.5 with dilute HCl, to enhance fibre-optic compatibility and MeOH solubility,[31] and to ensure that DCF is predominantly in its neutral form ($pK_a = 4.1$), favouring partitioning into the MIP phase and reproducible MIR absorption. Stock and working solutions were prepared in ultrapure water or MeOH and stored in amber glassware until use.

WSA Design and Operation

The Wastewater Spectroscopic Analyzer (WSA, Figure 1) comprises three integrated subsystems for autonomous water analysis: (i) multistage filtration (MSF) unit (three 5–10 μm pore size stages) developed by CYRIC, for remove of particulates and protection of the SPE cartridges, (ii) DCF-specific MIP-SPE cartridges (25 mg sorbent) for selective enrichment, and (iii) a mid-infrared quantum cascade laser (MIR-QCL) spectroscopy module targeting the DCF fingerprint region (1350–1660 cm^{-1}). The optical setup for field deployment employs a custom tunable Alpes Laser QCL module coupled via an $AgCl_{0.3}Br_{0.7}$ fibre-optic flow cell (5 cm pathlength, Art Photonics GmbH, Berlin) to a thermoelectrically cooled Vigo MCT detector. The transparent flow cell housing was 3D-printed using

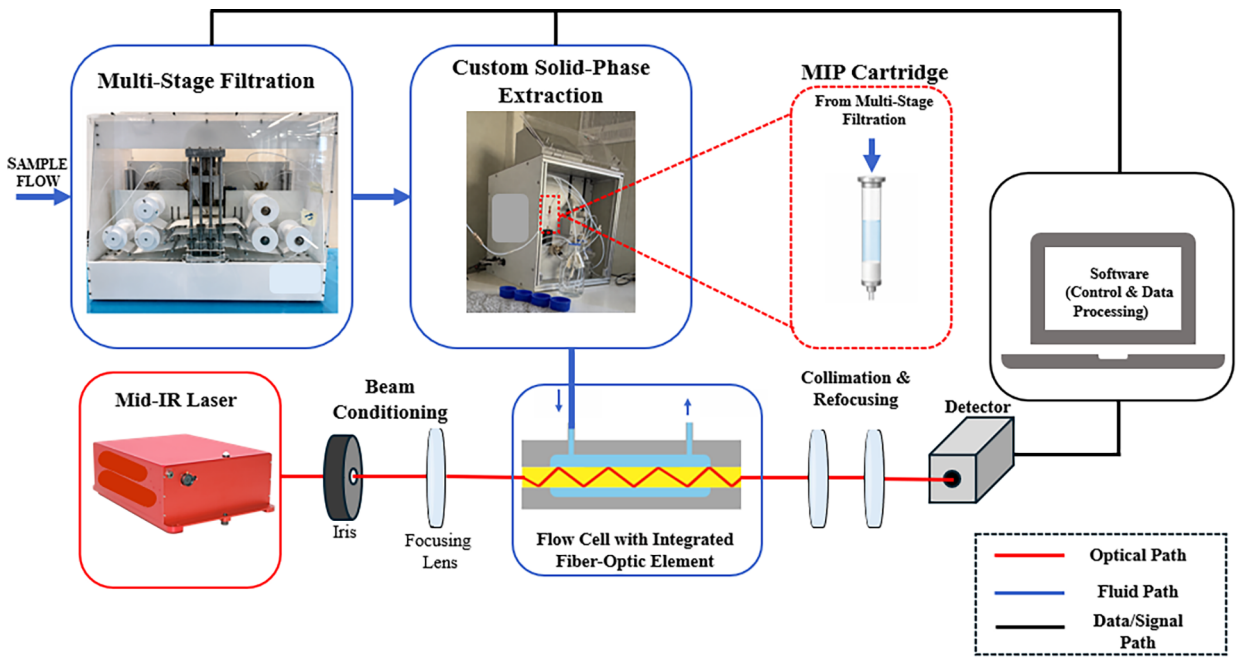

Figure 1. Schematic of the Wastewater Spectroscopic Analyzer integrating multi-stage filtration (MSF), customized solid phase extraction device with diclofenac-selective molecularly imprinted polymer cartridge, and a mid-infrared Alpes QCL optical unit. Raw wastewater flows sequentially through MSF → SPE → QCL sensor, yielding real-time DCF concentrations via the WebUI interface.

https://doi.org/10.1021/acssensors.6c01927
ACS Sens. XXXX, XXX, XXX−XXX

stereolithography (Formlabs Form 3 printer, 100 μm layer thickness, 405 nm curing wavelength), post-cured (UV at 60 °C for 30 min) and inspected to ensure clean internal channel. The MIR-QCL beam is coupled into a flexible $AgCl_{0.3}Br_{0.7}$ optical fibre waveguide immersed in the flow cell containing the methanolic MIP-SPE eluate. Due to the higher refractive index of the fibre compared with the surrounding liquid, the MIR radiation propagates via multiple total internal reflections along the fibre core, generating an evanescent wave that extends a few micrometres into the surrounding methanol solution at each reflection point. The diclofenac molecules present within this evanescent field selectively absorb radiation at their characteristic vibrational frequencies in the mid-infrared region, thereby attenuating the transmitted signal in proportion to their concentration. This fibre-optic attenuated total reflection (ATR) configuration allows the entire length of the fibre (5 cm) to act as a distributed multi-reflection detection element, thereby improving sensitivity compared with a single-pass transmission cuvette of equivalent physical length. A web-based user interface (WebUI) orchestrates operations: controlling MSF flow rate, MIP-SPE enrichment procedure with MeOH elution, spectral acquisition (1350–1660 cm^{-1}, 2 cm^{-1} resolution), and completing fully autonomous 120 min cycles.

Synthesis and Characterization of the Polymers

The diclofenac-selective molecularly imprinted polymer (MIP) was synthesized by bulk photopolymerization under UV irradiation (365 nm) for 16 h at room temperature using HPβCD-acrylate (HPβCD-Ac, 500 mg) as functional monomer, EGDMA (20 mmol) as crosslinker, the photoinitiator HCHPM (0.12 mmol) and DCF (0.2 mmol) as template, following our previously reported protocol for HPβCD-based porous polymers, with appropriate modifications for template incorporation.[32] After polymerization, the monolithic polymer was crushed and sieved to 25–100 μm particles, then exhaustively washed with MeOH/glacial acetic acid (9/1, v/v) and MeOH until no DCF was detected in the washings by UV-vis spectrophotometry, and dried in a vacuum oven overnight (50 °C, 600 mbar). A non-imprinted polymer (NIP) was prepared in parallel under identical conditions but without DCF. The polymers were characterized by Fourier-transform infrared spectroscopy (FTIR), nitrogen physisorption (BET surface area, pore volume), thermogravimetric analysis (TGA), scanning electron microscopy (SEM, Helios Nanolab 600, 5 kV, 86 pA), and elemental analysis, using the instrumentation detailed in ref 32.

DCF Preconcentration: MIP-SPE Development, Optimization, and Validation

MIP and NIP sorbents (25 mg) were packed into 3 mL SPE cartridges between polyethylene frits (20 μm porosity). A standardized four-step SPE protocol was used: (i) conditioning with MeOH/UPW, (ii) sample extraction/adsorption, (iii) MeOH elution/desorption, and (iv) cartridge regeneration/washing, with air-purge steps (5 mL at 10 mL min^{-1}) systematically applied between phases to eliminate cross-contamination and ensure reproducible performance. DCF calibration solutions were prepared in MeOH and by serial dilution from a methanolic stock solution in UPW/MeOH (99:1 v/v) and quantified by UV-Vis at λ_{max} = 277.5 nm (MeOH) and at λ_{max} = 276 nm (UPW/MeOH). Keys SPE performance metrics: equilibrium adsorption capacity (Q_e), extraction efficiency (EE), enrichment factor (EF), and recovery rate (R) were calculated using standard mass-balance equations (see Supporting Information for definitions and formulas). All experiments performed in triplicate and reported as mean ± SD. Preliminary one-factor-at-a-time (OFAT) optimization identified methanol as the optimal eluent (highest desorption efficiency) and neutral pH conditioning (maximal EE retention without DF precipitation complications at pK_a = 4.1). Subsequent design-of-experiments (DoE) optimization employed a three-level, four-factor Box–Behnken design (BBD) to simultaneously evaluate critical parameters (Table S1): adsorbent mass (X_1: 5–25 mg), sample loading flow rate (X_2: 1–5 mL min^{-1}), elution flow rate (X_3: 1–5 mL min^{-1}), and elution volume (X_4: 1–5 mL). The 27-run experimental matrix (81 total runs with triplicates, Table S2) targeted maximum EF response via second-order quadratic polynomial regression (eq S5), analyzed using STATGRAPHICS Centurion 19 software to generate a 3D response surface and ANOVA. To evaluate method sensitivity under dilute conditions, DCF working solutions at 0.1, 0.3, 1, 3, and 10 mg L^{-1} were applied to the optimized SPE setup and Q_e was determined for each concentration. Maximum adsorption capacity Q_m (mg g^{-1}) was determined from isotherm experiments using DCF solutions in the range 1–120 mg L^{-1}, with Q_e values fitted to the Langmuir model (eq 1):

$$Q_e = \frac{C_e K_L Q_m}{1 + C_e K_L} \quad (1)$$

and the Freundlich model (eq 2):

$$Q_e = K_F C_e^{1/n} \quad (2)$$

where K_L is the Langmuir constant (mg L^{-1}), and K_F (mg g^{-1}) and n are the constants of the Freundlich constants. A field emulation study was performed by processing 1 L of model solution spiked at 1500 ng L^{-1} DCF, with the input concentration independently verified by the accredited testing laboratory ZV Landeswasserversorgung (Betriebs- und Forschungslabor – organische Spurenanalytik, Zweckverband Landeswasserversorgung Langenau, Germany) in accordance with DIN EN ISO 21676:2022-01#. Method robustness was assessed through 10-cycle reusability testing with intermediate MeOH washing. Selectivity was evaluated against the structural analogues IBU, MFA, and NPX (Figure S1) using the selectivity factor (eq 3):

$$\alpha = \frac{EE_{analog}}{EE_{DF}} \quad (3)$$

where EE_{DF} (%) and EE_{analog} (%) are the extraction efficiencies for DCF and the respective analogue. UV–vis quantification of analogues was performed at their individual absorption maxima (in UPW/MeOH: IBU 221.5 nm, CBZ 285.0 nm, ASA 226.0 nm; in MeOH: IBU 220 nm, CBZ 285.0 nm, ASA 226 nm), with one pharmaceutical per SPE run to avoid spectral overlap.

Before field deployment, the preconcentration performance of the customized MIP-SPE cartridges was benchmarked against a commercial SPE reference under identical operating conditions. A model DCF solution (200,000 ng L^{-1} in UPW/MeOH 99:1 v/v) was processed through both sorbent types following the standardized four-step protocol described above (conditioning, loading, elution with 1 mL MeOH, regeneration). Eluates were quantified by UV–vis spectroscopy using the MeOH-matrix calibration curve (λ_{max} = 277.5 nm, using the calibration function C (mg L^{-1}) = 0.04748x + 0.00288) and EF was calculated via eq S3. For the customized MIP-SPE, experiments were performed in triplicate (runs 1–3) to evaluate reproducibility and cartridge-to-cartridge consistency. All results were reported as EF ± SD and compared directly to the commercial reference to identify any systematic or random deviations requiring further optimization before field integration.

Laboratory Setup, Spectral Validation, and Pre-Deployment Characterization of the QCL Sensor

The custom QCL sensor (see Figure 2) was validated in the laboratory prior to field deployment by (i) spectral comparison with a conventional attenuated total reflectance Fourier-transform infrared (ATR-FTIR) reference, and (ii) quantitative calibration to determine the method limit of detection (MLD) and quantification (MLQ), and linearity range. For spectral validation, DCF solutions in MeOH were introduced into the fibre-optic flow cell (0.88 ± 0.06 mL) and the resulting MIR-QCL spectrum was compared to the DCF powder

https://doi.org/10.1021/acssensors.6c01927
ACS Sens. XXXX, XXX, XXX–XXX

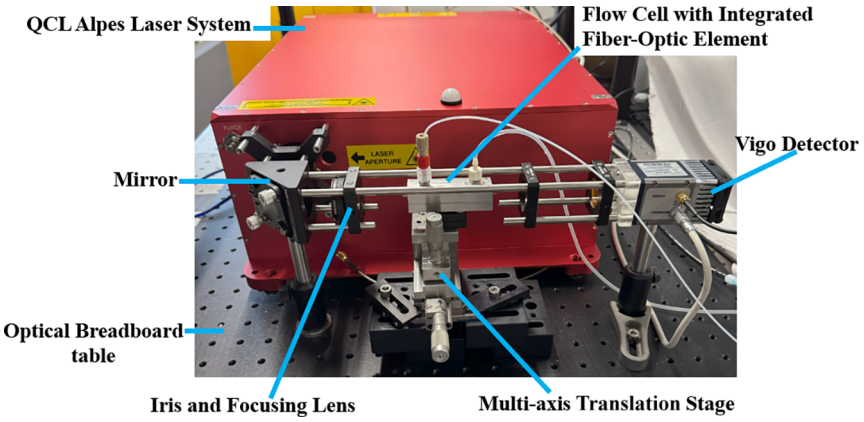

Figure 2. Laboratory-calibrated Alpes QCL spectroscopic sensor integrated with AgX fibre-optic flow cell (foreground) and VIGO detector, configured for WSA DCF quantification.

spectra acquired with a Bruker Alpha Platinum ATR-FTIR spectrometer (diamond crystal, 128 scans, 2 cm^{-1} resolution), focusing on the aromatic C≡C stretch around 1506 cm^{-1}, and carbonyl/C–N bands in the 1550–1650 cm^{-1} region. Agreement between the techniques was evaluated from the band pattern and the Pearson correlation coefficient over the 1350–1660 cm^{-1} window. For quantitative calibration, a series of DCF standards was measured under identical flow-cell conditions, and baseline-corrected absorbance at 1506 cm^{-1} was plotted versus concentration to assess linearity (R^2). The MLD and MLQ were calculated according to IUPAC guidelines (3σ/slope and 10σ/slope, respectively, where σ is the standard deviation of the blank).[33] Reproducibility was expressed as RSD (%) across triplicate measurements at each concentration level.

Field Deployment and Autonomous Monitoring Campaigns

Field validation of the full assembled WSA was conducted at pilot sites representative of distinct wastewater matrices: MITERA Hospital (clinical wastewater, Athens, Greece) and EYDAP Psyttalia WWTP (municipal influent, Greece). Complete WSA units were transported and installed in situ at both locations (Figure S2), with all subsystems (Cyric MSF, MIP-SPE, custom Alpes Laser) interconnected and configured for fully autonomous operation via the interface. Wastewater samples were collected and analyzed following a standardized A/B paired protocol: Sample A consisted of raw wastewater (50–100 mL) collected post-MSF filtration without MIP-SPE enrichment, serving as the unprocessed matrix reference; Sample B consisted of the 1 mL MeOH eluate obtained after MIP-SPE enrichment of the same wastewater volume under DoE-optimized conditions. Four sample pairs were analyzed across both sites (Table S3), comprising non-spiked native wastewater and 35 ng mL^{-1} DCF-spiked samples to assess recovery under field conditions. Each autonomous WSA cycle (120 min total duration) executed the following sequential workflow without operator intervention: automated sample intake → MSF pretreatment → MIP-SPE loading and enrichment with MeOH elution → QCL spectral acquisition (1350–1660 cm^{-1}). Real-time subsystem status (MSF flow rates, SPE cartridge back-pressure, QCL readiness, and spectral acquisition progress) was continuously monitored via the WebUI, and any deviations or automated alerts were logged in standardized field sheets for post-campaign traceability. Each WSA cycle result was benchmarked against external reference analysis performed by the Trace Analysis and Mass Spectrometry Group of the National and Kapodistrian University of Athens (TraMS/NKUA) laboratory using liquid chromatography/gas chromatography systems coupled with high-resolution mass spectrometry (LC/GC-HRMS/MS). Sample collection, preservation, transport, and chromatographic analysis followed accredited procedures detailed in Supporting Information (Text S1). Agreement between WSA and reference values was expressed as percentage deviation and used to assess trueness under authentic field conditions.

■ RESULTS AND DISCUSSION

Performance and Selectivity of DCF-Imprinted Polymers

SEM imaging and nitrogen physisorption (Figure 3) confirmed the expected morphological contrast between MIP and NIP: the MIP displayed an open, porous structure with template-extraction cavities, while NIP was denser and compact, consistent with successful molecular imprinting (Figure 3a,b).[31,34] Nitrogen physisorption confirmed the enhanced porosity of the MIP (Figure 3c). Despite its smaller overall surface area (31.14 m^2 g^{-1} vs 81.03 m^2 g^{-1} for NIP), the MIP exhibited a more uniform pore distribution centred around 15–18 Å, consistent with DCF-complementary cavities enhancing selective accessibility. The lower BET surface area of the MIP relative to the NIP reflects partial pore occupancy by the template during polymerization, which, upon extraction, yields a geometrically selective cavity architecture rather than maximizing total surface area, a well-documented feature of bulk-polymerized MIPs.[35] The chemical integrity of both MIP and NIP was confirmed by FT-IR, showing the characteristic bands of HPβCD-Ac (O–H at 3200–3600 cm^{-1}, C≡O at 1723 cm^{-1}, C–O at 1159 cm^{-1}). A specific band at 1460 cm^{-1} appeared only for the MIP, indicating template-induced structural rearrangements and confirming complete DCF removal (Figure S3a). Powder XRD confirmed the amorphous nature of both polymers (weak $2\theta = 15°$ peak attenuated in MIP; Figure S3b), consistent with the non-crystalline architecture typical of bulk-polymerized cyclodextrin-derived MIPs.[31]

Having confirmed the successful imprinting and structural integrity of the MIP through morphological and spectroscopic characterization, we next evaluated its functional performance by optimizing the elution conditions required to maximize DCF recovery. Among the solvents tested (see detailed comparison of extraction efficiency for ACN, MeOH, EtOH, DMSO, and DMF; Figure S4), methanol provided the highest desorption efficiency and was selected as the eluent for all subsequent experiments. The superior desorption efficiency of methanol can be rationalized by its intermediate polarity

https://doi.org/10.1021/acssensors.6c01927
ACS Sens. XXXX, XXX, XXX–XXX

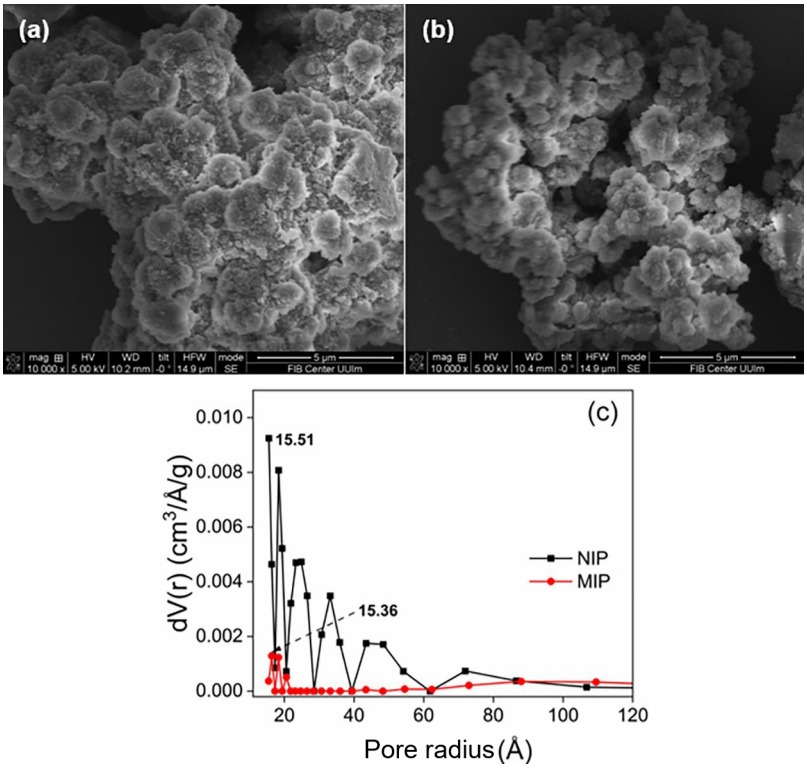

Figure 3. Morphological and porosity characterization of NIP and MIP. (a) SEM image (10,000×) of dense, aggregated NIP particles. Reproduced from ref 32. Available under CC-BY 4.0 licence. Copyright 2026 Huber et al. (b) SEM image (10,000×) of the open, porous MIP morphology with template-extraction cavities (this work). (c) Pore size distribution curves of NIP (black) and MIP (red, this work), based on N_2 adsorption–desorption isotherms measured at 77 K. NIP data reproduced from ref 32. Available under CC-BY 4.0 licence. Copyright 2026 Huber et al.

(dielectric constant ε = 32.7), which disrupts the hydrogen-bonding and hydrophobic interactions stabilizing DCF within the HPβCD-Ac cavity while remaining compatible with the polymer matrix. Solvents of higher polarity (DMF, ε = 36.7; DMSO, ε = 46.7; ACN, ε = 37.5) more strongly solvate DCF in bulk solution but limit diffusion into the hydrophobic imprinted cavities, whereas a less polar solvent (EtOH, ε = 24.6) provides insufficient disruption of the host-guest hydrogen-bonding network. The moderate polarity and small molecular size of methanol thus promote efficient penetration and the competitive displacement of DCF from the binding sites. Notably, the imprinting factor (IF = EF_{MIP}/EF_{NIP}) obtained using methanol was 1.39, confirming that the MIP exhibited selective binding toward the target analyte compared to the NIP under the chosen elution conditions. This IF value is in line with those reported for analogous DCF-MIP systems, where IF values in the range of 1.2–2.5 are typically observed for bulk-polymerized materials.[31,35] Consequently, all further experiments will be performed exclusively with the MIP. The effect of conditioning pH on MIP-SPE performance was evaluated at pH 2 and neutral pH (Table S4). While EE was high at both conditions (98.0 ± 3.3% at neutral pH vs 100.0% at pH 2), the recovery rate (42.1 ± 4.7% at pH 2 vs 99.3 ± 1.7% at neutral pH) and enrichment factor (EF = 4.21 ± 0.47 at pH 2 vs 9.96 ± 0.28 at neutral pH) dropped markedly under acidic conditioning. These results indicate that although DCF is efficiently loaded onto the MIP sorbent under both pH conditions, acidic conditioning strengthens DCF retention within the imprinted cavities likely through enhanced hydrogen-bonding and/or ionic interactions involving the protonated carboxylic acid group thereby impairing subsequent methanol-based elution. Neutral pH conditioning was therefore selected for all subsequent experiments, maximizing both adsorption capacity and, critically, recovery of the enriched analyte. A second-order polynomial model (eq 4) was fitted to the enrichment factor (EF) as a function of sorbent mass (X_1), sample flow rate (X_2), elution flow rate (X_3), and elution volume (X_4).

$$Y = 29.30 + 1.64X_1 - 1.023X_2 - 1.04X_3 - 15.35X_5 - 0.019X_1^2 + 0.013X_1X_2 + 0.004X_1X_3 - 0.221X_1X_4 + 0.166X_2^2 + 0.099X_2X_3 - 0.162X_2X_4 + 0.110X_3^2 + 0.013X_3X_4 + 2.166X_4^2 \quad (4)$$

The sign preceding each independent factor or quadratic or dual interaction term indicates the respective effect, with positive values indicating that an increase in their level results in an increase in response, and negative values indicating that an increase in their level results in a decrease in response. ANOVA (Table S5) confirmed excellent model fitness with ($R^2 = 0.974$, adjusted $R^2 = 0.967$). Sorbent mass (X_1) and elution volume (X_4) were the two most statistically influential parameters ($p < 0.0001$), with X_4 showing a strong nonlinear effect. The interaction term $X_1 \times X_4$ was also significant ($p < 0.0001$), indicating that the benefit of increasing sorbent mass is most pronounced at low elution volumes. This result highlights the critical role of the sorbent mass-to-elution volume ratio in governing enrichment, consistent with SPE theory and previously reported DoE studies on pharmaceutical MIP-SPE systems.[36] Flow rates (X_2, X_3) had limited individual influence on EF ($p > 0.15$).

https://doi.org/10.1021/acssensors.6c01927
ACS Sens. XXXX, XXX, XXX–XXX

Three-dimensional response surface plots and Pareto analysis confirm that EF increases with increasing sorbent mass and decreasing elution volume, while identifies sorbent mass and elution volume as the dominant factors governing enrichment factor ($R^2 = 0.974$, Table S5 and Figure S5), with optimal conditions of 25 mg sorbent, 5 mL min^{-1} sample flow rate, 1 mL min^{-1} elution flow rate, and 1 mL elution volume (predicted EF = 40.4, experimental EF = 39.4, relative deviation <3%). Under optimized conditions, the MIP-SPE achieved EE exceeding 98%, EF above 49, and recoveries higher than 98% across the calibration range of 0.1–10 mg L^{-1} (linear range, $y = (42.64 \pm 0.38)x + (0.90 \pm 0.15)$, $R^2 = 0.999$), with MLD = 10.55 ± 0.09 μg L^{-1} and MLQ = 35.18 ± 0.31 μg L^{-1} (Table S6 and Figure S6). These performance metrics compare favourably with previously reported DCF-MIP-SPE systems with reported recoveries of 82–88% in deionized water using a bulk-polymerized DCF-MIP.[31] Adsorption isotherm fitting (1–120 mg L^{-1} DCF, Figure S7) yielded maximum adsorption capacities of Q_m = 147.59 mg g^{-1} (Langmuir, K_L = 0.57 L mg^{-1}, $R^2 = 0.98$) and K_F = 66.33 mg g^{-1}, n = 5.39 (Freundlich, $R^2 = 0.82$), indicating that adsorption likely occurs predominantly as a monolayer on homogenous sites (preferential Langmuir behaviour).[37] In contrast, the Freundlich constants ($n > 1$) indicate favorable adsorption. Benchmarking against commercial C18 sorbents (Figure S8) confirmed significantly higher MIP adsorption (9.55 mg L^{-1} vs 5.94–6.93 mg L^{-1}) and higher recovered DCF concentrations, attributable to the cyclodextrin cavity-specific recognition mechanism unavailable in non-selective reverse-phase sorbents. This 37.8–60.8% enhancement in DCF adsorption relative to conventional non-selective C18 sorbents, combined with the 1.39-fold imprinting factor of observed relative to the NIP control, jointly demonstrates that the template cavity architecture and the imprinting process itself, rather than generic hydrophobic sorption, underlie the selective preconcentration performance of the MIP-SPE approach. After 10 adsorption–desorption cycles, the MIP retained most of its initial adsorption capacity (Figure S9), confirming reusability consistent with other pharmaceutical MIP-SPE sorbents reported in the literature and supporting the economic viability of the sorbent for repeated field deployment cycles.[36] At environmentally relevant concentrations (1 L, 1500 ng L^{-1} DCF), the MIP-SPE achieved EF = 565 ± 97, and a recovery of 56.5 ± 9.7%, confirming strong-trace level enrichment capability despite moderate recovery at high volume-to-mass ratios. Selectivity testing against structural analogues (IBU, MFA, and NPX, see Figure S10) showed near-complete co-extraction of IBU (EE = 95.5 ± 0.4%, selectivity factor α = 0.979) due to structural and physicochemical similarity with DCF, while MFA and NPX displayed markedly lower cross-reactivity (α = 0.084 and α = 0.194, respectively), consistent with a hydrophobic, shaped-selective recognition mechanism within the cyclodextrin based cavities. Benchmarking of customized fluidic SPE against commercial SPE cartridges (same MIP batch, 20,000 ng L^{-1} DCF) showed comparable EF magnitude but higher variability in the automated configuration (EF = 14.8 vs 27.6), attributable to fluidic engineering factors (flow distribution, back-pressure instabilities, and cartridge-seating) rather than sorbent limitations. Method precision, expressed as relative standard deviation (*RSD*) calculated from triplicate measurements, was excellent for calibration parameters and high-concentration selectivity tests (RSD = 0.2–0.9%), while the field-emulation enrichment experiment showed higher variability (RSD = 17.2%), consistent with the amplified sensitivity to loading conditions at trace-level concentrations and high sample volume-to-sorbent mass ratios discussed above.

Laboratory Validation of the MIR-QCL Sensor Performance

SEM imaging of the polished AgX fibre end-facet (Figure 4a) confirmed a smooth, defect-free surface essential for minimizing scattering losses and ensuring reproducible coupling efficiency. Visible light transmission through the 5 cm $AgCl_{0.3}Br_{0.7}$ fiber (Figure 4b) qualitatively confirmed efficient waveguiding. Quantitative transmission measurement at 1500 cm^{-1} (8 mW input, 2.2 mW output) yielded a transmission efficiency of ∼27% and an optical loss of ∼73%. This value falls within the 15–30% range reported for AgClBr fibers in mid-IR ATR/FTIR probe configurations by Damin and Sommer depending on coupling quality, fiber length, and alignment conditions, and is consistent with the ∼0.12 dB/cm loss reported for similar AgClBr polycrystalline fibers.[38,39]

Spectral comparison with the ATR-FTIR powder reference (Figure 5) confirmed correct identification of all major diagnostic bands (COO^- symmetric stretch at 1455 cm^{-1}, aromatic C≡C stretch at 1506 cm^{-1}, aromatic ring C≡C stretch between 1538–1558 cm^{-1}, and C≡O stretch between 1546 cm^{-1}).[40,41] The linear absorbance increase with concentration confirms Beer–Lambert compliance through the AgX fiber-optic flow cell. The Pearson correlation coefficient between normalized QCL and ATR-FTIR absorbance profiles across the 1350–1660 cm^{-1} window was $r = 0.974$ ($n = 119$, $p < 10^{-50}$), confirming high spectral fidelity of the MIR-QCL sensor and validating its use for quantitative DCF fingerprinting.

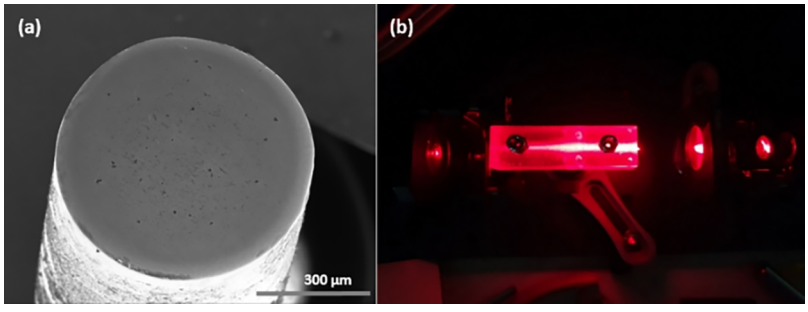

Figure 4. (a) SEM image of polished AgX fiber end-facet; (b) visible light transmission through a 5 cm AgX fiber illuminated by LED in darkness.

https://doi.org/10.1021/acssensors.6c01927
ACS Sens. XXXX, XXX, XXX–XXX

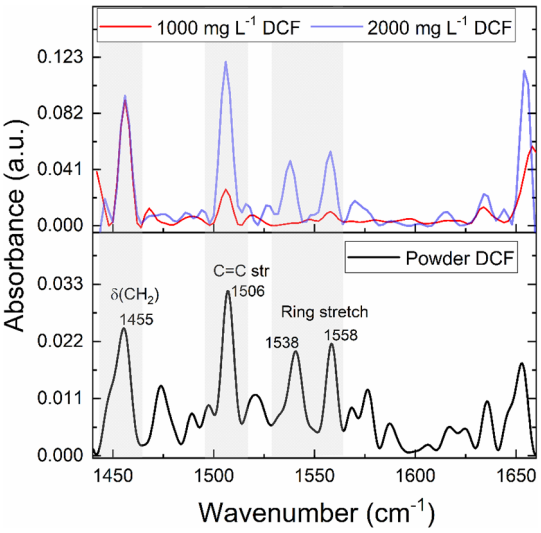

Figure 5. DCF infrared spectra: ATR-FTIR reference (black, powder; 2 cm^{-1}, 128 scans) vs Alpes QCL custom sensor (red: 1000 mg L^{-1}, blue: 2000 mg L^{-1} in MeOH; AgX fiber Ø700 μm, length 5 cm; resolution 2 cm^{-1}).

Calibration revealed two distinct linearity regimes: a high sensitivity low-concentration range (1–30 mg L^{-1}, MLD = 0.60 mg L^{-1}, MLQ = 1.82 mg L^{-1}) and an extended high-concentration range (30–300 mg L^{-1}, MLD = 14.33 mg L^{-1}, MLQ = 47.77 mg L^{-1}), confirming robust linearity across three orders of magnitude without signal saturation (Figure 6 and Table S7). Notably, this QCL-alone MLD (0.60 mg L^{-1}) is substantially higher than the MLD achieved by the MIP-SPE preconcentration step measured independently by UV-Vis (10.55 μg L^{-1}), indicating that the mid-infrared detection stage rather than the sorbent chemistry constitutes the sensitivity-limiting component of the integrated WSA workflow. While the spectroscopic MLD is high than UV-Vis (0.132 mg L^{-1}), the QCL sensor provides complementary molecular fingerprint specificity essential for unambiguous DCF identification in complex MIP eluates.

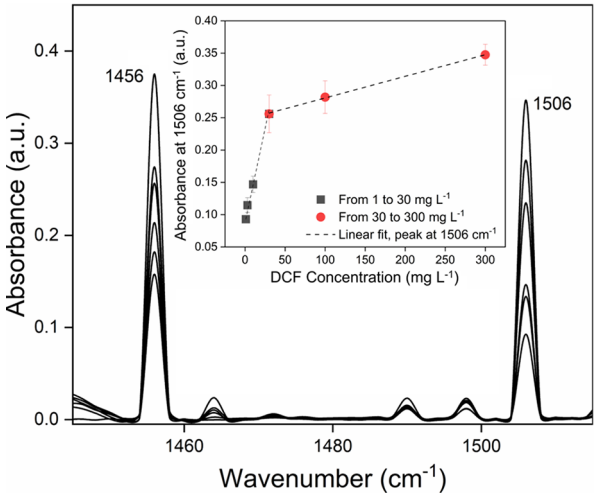

Figure 6. QCL infrared spectra of DCF in MeOH from 3–100 mg L^{-1} (AgX fiber Ø 700 μm, length 5 cm). Insets: corresponding calibration curves at 1506 cm^{-1}.

Field Deployment and Real-World Validation

The WSA (instrumental MLD: 600 ng mL^{-1}) was benchmarked against LC/GC-HRMS/MS reference analysis (MLD 0.071 ng mL^{-1}) across four sample pairs from MITERA hospital and EYDAP Psyttalia WWTP (Table 1). The large MLD gap underscores the essential role of the MIP-SPE enrichment in bridging sensitivity for early-warning applications rather than trace-level reference analysis. It is acknowledged that the current validation dataset (n = 4 sample pairs across two sites) constitutes a proof-of-concept demonstration at TRL 6–7. Excellent agreement was obtained for enriched samples (Table 1): Sample 2B (EF = 97.4) showed 91% agreement (2175 vs 2386 ng mL^{-1}), and Sample 3B (EF = 1004.8) showed 92% agreement (2617 vs 2274 ng mL^{-1}), both within the ±20% tolerance accepted under ISO/IEC 17025 for environmental water analysis (Figure 7).[17] Sample 1B showed a larger deviation at extreme enrichment factor (EF = 12,433), attributable to amplified variability at very high EF, while Sample 4B (WSA: n.d. vs reference = 846 ng mL^{-1}) identifies the current WSA MLD limitation (600 ng mL^{-1} post-enrichment) for low-DCF municipal matrices. Parallel multi-pollutant screening (12 pharmaceuticals and 2 benzotriazoles) (Table S8) confirmed strong DCF selectivity in real matrices: DCF dominated post-enrichment composition across all hospital samples (75–85% of total pharmaceuticals and personal care products (PPCP) content, 2274–3009 ng mL^{-1}), with a 3–35-fold DCF/carbamazepine selectivity ratio, validating targeted enrichment for EU Water Framework Directive/Watch List-compliant DCF surveillance.

To contextualize the analytical performance of the proposed WSA, a comparative summary against previously reported diclofenac monitoring methods is provided in Table S9. While immunoassay- and MS-based techniques offer superior sensitivity, and electrochemical sensors provide faster, low-cost alternatives, none have demonstrated autonomous field deployment. In contrast, the WSA integrates MIP-SPE preconcentration and MIR-QCL detection into a single field-validated platform, achieving 91–92% agreement with reference LC/GC-HRMS/MS methods at approximately 50-fold faster turnaround than conventional laboratory workflows.

Implications for Autonomous Pharmaceutical Surveillance

Future WSA development will target three priority areas directly motivated by the limitations identified in the current field validation. First, municipal MLD reduction below 600 ng mL^{-1} will be pursued through distributed feedback (DFB) QCL implementation (linewidth < 0.001 cm^{-1}), with dual-cavity feedback stabilization and phase-sensitive lock-in amplification of the modulated QCL signal projected to achieve 5–10× SNR improvement, pushing the effective instrumental MLD to 100–200 ng mL^{-1} while maintaining 1506 cm^{-1} DCF specificity. Second, multi-reflection ATR cells (5–10× pathlength gain) will amplify mid-IR absorbance through increased effective pathlength, while hybrid DCF-MIP sorbents synergistically combining cavity-specific recognition with high-capacity metal-organic framework adsorption are expected to stabilize EF across the 100–12,000-fold range observed in field campaigns and reduce inter-sample variability and cartridge-to cartridge

https://doi.org/10.1021/acssensors.6c01927
ACS Sens. XXXX, XXX, XXX–XXX

Table 1. DCF Quantification: WSA Sensor vs External Laboratory Analysis[a]

sample	WSA (ng mL^{-1})	external lab (ng mL^{-1})	agreement	notes
1A	n.a.	0.24		background level, below WSA MLD
1B	1000 ± 50	3009		EF = 12433.0; extreme enrichment
2A	n.a.	24.5		background level
2B	2175 ± 70	2386	91%	EF = 97.4, spiked hospital
3A	n.a.	2.27		low native DCF
3B	2617 ± 100	2274	92%	EF = 1004.8, non-spiked hospital
4A	n.a.	1.66		low native
4B	n.d	846		EF = 509.6, non-spiked sample
instrumental MLD	600	0.071		

[a]EF: Enrichment Factor, n.a.: not analyzed, n.d.: not detected, MLD: Method limit of detection.

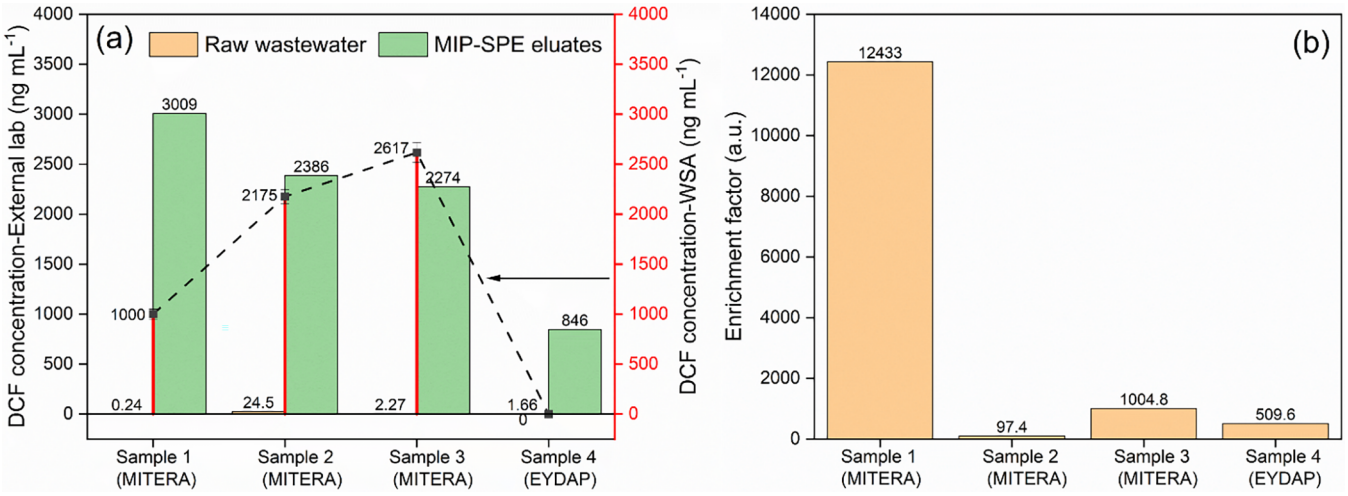

Figure 7. Diclofenac enrichment by MIP-SPE during field deployment: (a) DCF concentrations in raw wastewater (measured by the external laboratory) and MIP-SPE eluates (measured by the WSA and the external laboratory); (b) corresponding enrichment factors across authentic wastewater samples, based on the external laboratory results.

drift in EF.[32–37,39,42–45] Third, machine learning-based spectral deconvolution will enable rejection of co-extracted PPCP signals (carbamazepine, metoprolol signals) at sub-10 ng mL^{-1},[46–48] alongside WebUI predictive analytics for real-time EF estimation and automated cartridge switching supporting continuous 24/7 monitoring under dynamically varying wastewater matrices. These incremental TRL 8-9 advancements build directly on demonstrated field-validated performance (91–92% HRMS agreement), positioning WSA for regulatory-compliant, autonomous pharmaceutical surveillance across EU wastewater networks in support of Water Framework Directive implementation and emerging pharmaceutical monitoring obligations.

■ CONCLUSIONS

This study demonstrates that the wastewater spectroscopic analyzer can reliably perform autonomous, field-deployable monitoring of diclofenac in complex wastewater matrices using mid-infrared QCL spectroscopy coupled to a selective HPβCD-based MIP-SPE preconcentration unit. Across authentic hospital and municipal samples, the system delivered enrichment factors up to 10^3, achieved 91–92% agreement with accredited LC/GC-HRMS/MS measurements, and completed multiple 120 min unattended operating cycles, corresponding to TRL 6–7 performance for continuous pharmaceutical surveillance. Beyond establishing analytical feasibility, the results show that integrating molecularly imprinted enrichment with molecular-fingerprint MIR detection can shift diclofenac monitoring from episodic, laboratory-based analysis to on-site, near–real-time measurement with substantially reduced operating cost and complexity. Remaining challenges include lowering the effective field method limit of detection for low-level municipal effluents and expanding validation across broader temporal and spatial scales. Addressing these through advances in laser architecture, sorbent design, and data analytics will position the platform as a scalable blueprint for autonomous early-warning networks targeting EU Water Framework Directive priority pharmaceuticals in wastewater.

■ ASSOCIATED CONTENT

Supporting Information

The Supporting Information is available free of charge at https://pubs.acs.org/doi/10.1021/acssensors.6c01927.

Experimental details and reagents; Box–Behnken design optimization of the SPE process (Tables S1, S2, S4, S5, Figure S5); pharmaceutical structures and WSA field-deployment details (Figures S1, S2, Text S1); polymer

https://doi.org/10.1021/acssensors.6c01927
ACS Sens. XXXX, XXX, XXX–XXX

characterization, eluent optimization, calibration, and adsorption isotherms (Figures S3, S4, S6, S7, Table S6); benchmarking, reusability, and selectivity of the MIP (Figures S8–S10); QCL sensor performance (Table S7); external laboratory analyte screening (Table S8); and comparison of analytical methods for diclofenac monitoring in water/wastewater (Table S9) (PDF)

AUTHOR INFORMATION

Corresponding Authors

Sherman Lesly Zambou Jiokeng – *Institute of Analytical and Bioanalytical Chemistry, Ulm University, Albert-Einstein-Allee 11, 89081 Ulm, Germany;* orcid.org/0000-0002-3279-8139; Email: sherman.jiokeng-zambou@uni-ulm.de

Boris Mizaikoff – *Institute of Analytical and Bioanalytical Chemistry, Ulm University, Albert-Einstein-Allee 11, 89081 Ulm, Germany;* orcid.org/0000-0002-5583-7962; Email: boris.mizaikoff@uni-ulm.de

Authors

Dionysis Adamou – *CY.R.I.C Cyprus Research and Innovation Center Ltd, 2643 Nicosia, Cyprus*

Amelie Huber – *Institute of Analytical and Bioanalytical Chemistry, Ulm University, Albert-Einstein-Allee 11, 89081 Ulm, Germany*

Lauralie Debard – *Institute of Analytical and Bioanalytical Chemistry, Ulm University, Albert-Einstein-Allee 11, 89081 Ulm, Germany*

Giorgos Katsouras – *Athens Water Supply and Sewerage Company S.A (EYDAP), Research and Development, 156 Oropou Str., 11146 Athens, Greece;* orcid.org/0000-0003-3249-3113

Panagiotis Georgiadis – *Alpes Lasers SA, 2072 St. Blaise, Switzerland*

Miltiadis Vasileiadis – *Alpes Lasers SA, 2072 St. Blaise, Switzerland*

Anthi Yfanti – *Athens Water Supply and Sewerage Company S.A (EYDAP), Research and Development, 156 Oropou Str., 11146 Athens, Greece*

Zoe Zacharouli – *MHTERA Hospital, 6, Erythrou Stavrou Str., Marousi, 15123 Athens, Greece*

Panagiotis Margaritis – *MHTERA Hospital, 6, Erythrou Stavrou Str., Marousi, 15123 Athens, Greece*

Complete contact information is available at: https://pubs.acs.org/doi/10.1021/acssensors.6c01927

Author Contributions

The manuscript was written through contributions of all authors. All authors have given approval to the final version of the manuscript.

Notes

The authors declare no competing financial interest.

ACKNOWLEDGMENTS

This work was funded by the EU Horizon 2020 project ENVIROMED (Grant No. 101057844), which focuses on developing a next-generation toolbox for greener pharmaceutical design and manufacturing to reduce environmental impact. We thank the Open Access Publishing Fund of the University of Ulm for funding. Special thanks are extended to Dr. Gregor Neusser at the Focused Ion Beam Center UUlm (Institute of Analytical and Bioanalytical Chemistry, Ulm University, Germany) for assistance with the SEM studies and to Dipl.-Ing. (FH) Sabine Junginger at ZV Landeswasserversorgung (Betriebs- und Forschungslabor – organische Spurenanalytik, Zweckverband Landeswasserversorgung Langenau, Germany). We thank Dr. Dimitrios Triantafyllos Gerokonstantis and the Trace Analysis and Mass Spectrometry Group, National and Kapodistrian University of Athens, for performing the LC-MS/MS analyses of pharmaceuticals in wastewater.

REFERENCES

(1) Jiokeng, S. L. Z.; Tonle, I. K.; Walcarius, A. Amino-Attapulgite/Mesoporous Silica Composite Films Generated by Electro-Assisted Self-Assembly for the Voltammetric Determination of Diclofenac. *Sens. Actuators B Chem.* **2019**, *287*, 296–305.

(2) Iula, G.; Raucci, A.; Antonelli, L.; Kalligosfyri, P. M.; De Cesaris, M. G.; Felli, N.; Natale, C. Di; Cinti, S.; Gentili, A. Smart and Sustainable 3D-Printed Electrochemical Device for Diclofenac Remediation and Monitoring in Water. *Talanta* **2026**, *297*, 128597.

(3) Al-Rajab, A. J.; Sabourin, L.; Lapen, D. R.; Topp, E. The Non-Steroidal Anti-Inflammatory Drug Diclofenac Is Readily Biodegradable in Agricultural Soils. *Sci. Total Environ.* **2010**, *409* (1), 78–82.

(4) Goodarzian, M.; Khalilzade, M. A.; Karimi, F.; Kumar Gupta, V.; Keyvanfard, M.; Bagheri, H.; Fouladgar, M. Square Wave Voltammetric Determination of Diclofenac in Liquid Phase Using a Novel Ionic Liquid Multiwall Carbon Nanotubes Paste Electrode. *J. Mol. Liq.* **2014**, *197*, 114–119.

(5) Baig, Z. T.; Ali, J.; Ali, A.; Naz, A.; Batool, M.; Shah, M. S.; Santali, E. Y. Isolation and Chemical Modification of Cellulose from Wheat Straw for the Removal of Diclofenac Potassium from Wastewater. *Emergent Mater.* **2024**, *8*, 61–74.

(6) Ali, A. M.; Rønning, H. T.; Sydnes, L. K.; Alarif, W. M.; Kallenborn, R.; Al-Lihaibi, S. S. Detection of PPCPs in Marine Organisms from Contaminated Coastal Waters of the Saudi Red Sea. *Sci. Total Environ.* **2018**, *621*, 654–662.

(7) Azzouz, A.; Jurado-Sánchez, B.; Souhail, B.; Ballesteros, E. Simultaneous Determination of 20 Pharmacologically Active Substances in Cow's Milk, Goat's Milk, and Human Breast Milk by Gas Chromatography-Mass Spectrometry. *J. Agric. Food Chem.* **2011**, *59* (9), 5125–5132.

(8) Yilmaz, B.; Ciltas, U. Determination of Diclofenac in Pharmaceutical Preparations by Voltammetry and Gas Chromatography Methods. *J. Pharm. Anal.* **2015**, *5* (3), 153–160.

(9) Elkady, E. F. Simultaneous Determination of Diclofenac Potassium and Methocarbamol in Ternary Mixture with Guaifenesin by Reversed Phase Liquid Chromatography. *Talanta* **2010**, *82* (4), 1604–1607.

(10) Theia'a, N. A. S.; Intisar, A. A. Spectrofluorimetric Determination of Propranolol and Diclofenac Medicines Using Fluorescein Dye. *J. Anal. Chem.* **2023**, *78* (Suppl 1), S26–S34.

(11) Hidalgo, J.; Fort, C. I.; Galambos, I.; Jankovics, H.; Hidalgo, L.; Turdean, G. L. TiO_2 Aerogel – A Sensing Electrode Matrix for the Sensitive Detection of Diclofenac Sodium. *Microchem. J.* **2024**, *207*, 111855.

(12) Bai, X.; Gao, W.; Zhou, C.; Zhao, D.; Zhang, Y.; Jia, N. Photoelectrochemical Determination of Diclofenac Using Oriented Single-Crystalline TiO_2 Nanoarray Modified with Molecularly Imprinted Polypyrrole. *Microchim. Acta* **2022**, *189* (3), 90.

(13) Ahmed, A. M. S.; Radalla, A. M.; Mohamed, M. A.; Mahmoud, R.; Farghali, A. A.; Hassouna, M. E. M. Green Voltammetric Method for Determination of Diclofenac Sodium in Environmental and Biological Samples Using Aluminium Tungstate Nanoparticles

Modified Carbon Paste Electrode. *Int. J. Environ. Anal. Chem.* **2024**, *105*, 4071–4090.
(14) Wang, Q.; Jiang, M.; Zhang, L. Label-Free and Visible-Light Driven Photoelectrochemical Sensor with CuCo2O4@CoO Core-Shell Hybrid Rod as Photoanode for Selective Sensing Diclofenac. *Electrochim. Acta* **2021**, *397*, 139239.
(15) Petruleviciene, M.; Savickaja, I.; Kovger-Jarosevic, J.; Skruodiene, M.; Juodkazyte, J.; Ramanavicius, S.; Ramanavicius, A. $BiVO_4$-Based Photoelectrochemical Sensors for the Detection of Diclofenac: The Role of Doping, Electrolytes and Applied Potentials. *Chemosensors* **2024**, *12* (12), 249.
(16) Garg, R.; Alattar, B.; Sabouni, R.; Ghommem, M. "Turn-on" Fluorescence-Based Diclofenac Detection Using Metal-Organic Framework-Coated Silicon Micropillars. *J. Water Process Eng.* **2025**, *76* (2), 108240.
(17) Mazouzi, Y.; Miche, A.; Loiseau, A.; Beito, B.; Méthivier, C.; Knopp, D.; Salmain, M.; Boujday, S. Design and Analytical Performances of a Diclofenac Biosensor for Water Resources Monitoring. *ACS Sens.* **2021**, *6* (9), 3485–3493.
(18) Mizaikoff, B. Infrared Optical Sensors for Water Quality Monitoring. *Water Sci. Technol.* **2003**, *47* (2), 35–42.
(19) Teuber, A.; Caniglia, G.; Wild, M.; Godejohann, M.; Kranz, C.; Mizaikoff, B. Espresso Science: Laser-Based Diamond Thin-Film Waveguide Sensors for the Quantification of Caffeine. *ACS Sens.* **2023**, *8* (5), 1871–1881.
(20) Rodionova, O. Y.; Titova, A. V.; Demkin, N. A.; Balyklova, K. S.; Pomerantsev, A. L. Qualitative and Quantitative Analysis of Counterfeit Fluconazole Capsules: A Non-Invasive Approach Using NIR Spectroscopy and Chemometrics. *Talanta* **2019**, *195*, 662–667.
(21) Fahelelbom, K. M. S.; Saleh, A.; Mansour, R.; Sayed, S. First Derivative ATR-FTIR Spectroscopic Method as a Green Tool for the Quantitative Determination of Diclofenac Sodium Tablets. *F1000Research* **2020**, *9*, 176.
(22) Nugrahani, I.; Dillen, N. Rapid Assay Development of Diclofenac Sodium Coated Tablet Assay Using FTIR Compared to HPLC Method. *Int. J. App. Pharm.* **2018**, *10* (4), 43–50.
(23) Haas, J.; Mizaikoff, B. Advances in Mid-Infrared Spectroscopy for Chemical Analysis. *Annu. Rev. Anal. Chem.* **2016**, *9*, 45–68.
(24) Teuber, A.; Mizaikoff, B. Cascade Laser Infrared Spectroscopy. *Encyclopedia of Analytical Chemistry*; Wiley, **2021**; pp 1–45.
(25) Haas, J.; Mizaikoff, B.; Fabrik, C.; Gmbh, K. B.; Mizaikoff, B. Advances in Mid-Infrared Spectroscopy for Chemical Analysis. *Annu. Rev. Anal. Chem.* **2016**, *9*, 45–68.
(26) Teuber, A.; Stach, R.; Haas, J.; Mizaikoff, B. Innovative Substrate-Integrated Hollow Waveguide Coupled Attenuated Total Reflection Sensors for Quantum Cascade Laser Based Infrared Spectroscopy in Harsh Environments. *Appl. Spectrosc.* **2022**, *76* (1), 132–140.
(27) Haas, J.; Catalán, E. V.; Piron, P.; Karlsson, M.; Mizaikoff, B. Infrared Spectroscopy Based on Broadly Tunable Quantum Cascade Lasers and Polycrystalline Diamond Waveguides. *Analyst* **2018**, *143* (21), 5112–5119.
(28) Stach, R.; Mizaikoff, B. Fuel Performance Specifications, Mid-Infrared Analysis of. *Encyclopedia of Analytical Chemistry*; Wiley, **2017**; pp 1–16.
(29) Daunis, T. B.; Dussor, J. C.; Le, B.; Hodges, K.; Clark, K. P.; Robbins, D. I.; Roodenko, K. Towards Infrared Photonic Integrated Circuits (PICs) in Biochemical Analysis: Implementation of Quantum Cascade Lasers (QCLs) in Analysis of Fluids. In *Optical Fibers and Sensors for Medical Diagnostics, Treatment and Environmental Applications XXII*, **2022**, vol *11953*; pp 50–58.
(30) Morales-Rodriguez, M. E.; McFarlane, J.; Kidder, M. K. Quantum Cascade Laser Infrared Spectroscopy for Online Monitoring of Hydroxylamine Nitrate. *Int. J. Anal. Chem.* **2018**, *2018* (1), 7896903.
(31) Samah, N. A.; Sánchez-Martín, M. J.; Sebastián, R. M.; Valiente, M.; López-Mesas, M. Molecularly Imprinted Polymer for the Removal of Diclofenac from Water: Synthesis and Characterization. *Sci. Total Environ.* **2018**, *631–632*, 1534–1543.
(32) Huber, A.; Rajpal, S.; Adamou, D.; Demosthenous, P.; Parlak, B.; Onel, S.; Mizaikoff, B.; Jiokeng, S. L. Z. Supramolecular β-Cyclodextrin Porous Framework for Selective Extraction of Diclofenac from Environmental Waters. *Microchem. J.* **2026**, *224*, 117712.
(33) Byrne, F. P.; Jin, S.; Paggiola, G.; Petchey, T. H. M.; Clark, J. H.; Farmer, T. J.; Hunt, A. J.; Robert McElroy, C.; Sherwood, J. Tools and Techniques for Solvent Selection: Green Solvent Selection Guides. *Sustain. Chem. Process.* **2016**, *4* (1), 7.
(34) Cantarella, M.; Carroccio, S. C.; Dattilo, S.; Avolio, R.; Castaldo, R.; Puglisi, C.; Privitera, V. Molecularly Imprinted Polymer for Selective Adsorption of Diclofenac from Contaminated Water. *Chem. Eng. J.* **2019**, *367* (1), 180–188.
(35) Meléndez-Marmolejo, J.; Díaz de León-Martínez, L.; Galván-Romero, V.; Villarreal-Lucio, S.; Ocampo-Pérez, R.; Medellín-Castillo, N. A.; Padilla-Ortega, E.; Rodríguez-Torres, I.; Flores-Ramírez, R. Design and Application of Molecularly Imprinted Polymers for Adsorption and Environmental Assessment of Anti-Inflammatory Drugs in Wastewater Samples. *Environ. Sci. Pollut. Res.* **2022**, *29* (30), 45885–45902.
(36) Nxumalo, N. L.; Mahlambi, P. N. Molecularly Imprinted Polymer-Based Adsorbents for the Selective Removal of Pharmaceuticals from Wastewater: Adsorption Kinetics, Isotherms, and Thermodynamics Studies. *Ind. Eng. Chem. Res.* **2023**, *62* (41), 16525–16544.
(37) Mpupa, A.; Dinc, M.; Mizaikoff, B.; Nomngongo, P. N. Exploration of a Molecularly Imprinted Polymer (MIPs) as an Adsorbent for the Enrichment of Trenbolone in Water. *Process* **2021**, *9* (2), 186.
(38) Damin, C. A.; Sommer, A. J. Characterization of Silver Halide Fiber Optics and Hollow Silica Waveguides for Use in the Construction of a Mid-Infrared Attenuated Total Reflection Fourier Transform Infrared (ATR FT-IR) Spectroscopy Probe. *Appl. Spectrosc.* **2013**, *67* (11), 1252–1263.
(39) Rave, E.; Nagli, L.; Katzir, A. Ordered Bundles of Infrared-Transmitting AgClBr Fibers: Optical Characterization of Individual Fibers. *Opt. Lett.* **2000**, *25* (17), 1237–1239.
(40) Ramachandran, E.; Ramukutty, S. Growth, Morphology, Spectral and Thermal Studies of Gel Grown Diclofenac Acid Crystals. *J. Cryst. Growth* **2014**, *389*, 78–82.
(41) Bouchal, R.; Miletto, I.; Thach, U. D.; Prelot, B.; Berlier, G.; Hesemann, P. Ionosilicas as Efficient Adsorbents for the Separation of Diclofenac and Sulindac from Aqueous Media. *New J. Chem.* **2016**, *40* (9), 7620–7626.
(42) Markham, S. K.; Mani, A.; Korsakova, E. A.; Korsakov, A. S.; Zhukova, L. V.; Bauer, J.; Silien, C.; Tofail, S. A. M. Polarisation Changes in Guided Infrared Thermography Using Silver Halide Poly-Crystalline Mid-Infrared Fibre Bundle. *J. Therm. Anal. Calorim.* **2020**, *142* (2), 1115–1122.
(43) Lux, L.; Phal, Y.; Hsieh, P. H.; Bhargava, R. On the Limit of Detection in Infrared Spectroscopic Imaging. *Appl. Spectrosc.* **2022**, *76* (1), 105–117.
(44) Madikizela, L. M.; Chimuka, L. Determination of Ibuprofen, Naproxen and Diclofenac in Aqueous Samples Using a Multi-Template Molecularly Imprinted Polymer as Selective Adsorbent for Solid-Phase Extraction. *J. Pharm. Biomed. Anal.* **2016**, *128*, 210–215.
(45) Anfossi, L.; Cavalera, S.; Di Nardo, F.; Spano, G.; Giovannoli, C.; Baggiani, C. Delayed Addition of Template Molecules Enhances the Binding Properties of Diclofenac-Imprinted Polymers. *Polymers* **2020**, *12* (5), 1178.
(46) Mokari, A.; Guo, S.; Bocklitz, T. Exploring the Steps of Infrared (IR) Spectral Analysis: Pre-Processing, (Classical) Data Modelling, and Deep Learning. *Mol.* **2023**, *28* (19), 6886.
(47) Rath, D.; Mikerásek, V.; Wang, C.; Eder, M.; Schmid, M.; Diebold, U.; Parkinson, G. S.; Pavelec, J. Infrared Reflection Absorption Spectroscopy Setup with Incidence Angle Selection for Surfaces of Non-Metals. *Rev. Sci. Instrum.* **2024**, *95* (6), 65106.
(48) Molnar, M.; Reardon, K. P.; Osborne, C.; Milić, I. Spectral Deconvolution With Deep Learning: Removing the Effects of Spectral PSF Broadening. *Front. Astron. Sp. Sci.* **2020**, *7*, 548909.